Spatial Waves in Synthetic Biochemical Networks

Adrien Padirac,[†] Teruo Fujii,[†] André Estévez-Torres,*,[‡] and Yannick Rondelez*,[†]

[†]LIMMS/CNRS-IIS, The University of Tokyo, Komaba 4-6-2, Meguro-ku, Tokyo 153-8505, Japan
[‡]Laboratoire de Photonique et de Nanostructures, CNRS, route de Nozay, 91460 Marcoussis, France

Ⓢ *Supporting Information*

ABSTRACT: We report the experimental observation of traveling concentration waves and spirals in a chemical reaction network built from the bottom up. The mechanism of the network is an oscillator of the predator–prey type, and this is the first time that predator–prey waves have been observed in the laboratory. The molecular encoding of the nonequilibrium behavior relies on small DNA oligonucleotides that enforce the network connectivity and three purified enzymes that control the reactivity. Wave velocities in the range 80–400 μm min^{-1} were measured. A reaction–diffusion model in quantitative agreement with the experiments is proposed. Three fundamental parameters are easy to tune in nucleic acid reaction networks: the topology of the network, the rate constants of the individual reactions, and the diffusion coefficients of the individual species. For this reason, we expect such networks to bring unprecedented opportunities for assaying the principles of spatiotemporal order formation in chemistry.
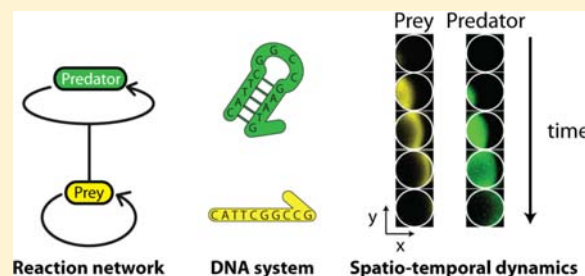
INTRODUCTION

Biological systems build themselves through a bottom-up process based on microscopic chemical interactions. Defining how macroscopic spatiotemporal order arises from cross-interacting chemical elements is a very basic step in the understanding of biological morphogenesis. In this quest, one approach is to dissect the molecular basis of morphogenesis directly within living systems.[1] However, despite great advances in the last two decades, experimental characterization of chemical reaction networks within living systems remains challenging.[2] A complementary approach seeks to synthesize sets of chemical reactions in vitro as more tractable models of biologically relevant pattern-forming processes. The recent emergence of methods to design and synthesize chemical reaction networks from the bottom up using nucleic acids has opened new doors in this direction.[3] In these synthetic systems, an arbitrary network of chemical interactions is rationally assembled, and the chemical parameters (rate constants and diffusion coefficients) can be quantitatively measured[4] and even tuned.[5] This bottom-up approach has two essential advantages. First, by releasing the constraints imposed by evolution on biological reaction networks, one may bring to light the universal processes that underlie pattern formation in biology. Second, learning how to obtain specific spatiotemporal behaviors from synthetic networks may reveal new ways of controlling matter at the molecular scale.

In this paper we demonstrate for the first time the de novo synthesis of traveling and spiral waves of concentration in a spatially extended and closed reactor. By "de novo" we mean that the molecular building blocks used here are classic enzymatic and DNA hybridization reactions that do not individually generate unusual nonlinear behaviors and that such behaviors are observed only when these reactions are connected in a precise way. We follow a modular approach that facilitates the experimental implementation of different circuits with a variety of nonequilibrium behaviors, such as relaxation oscillators[3d] and multistable switches.[3f] The molecular encoding of the nonequilibrium behavior relies on small DNA oligonucleotides that enforce the network connectivity and three purified enzymes that control the reactivity. In this work, the target mechanism is an oscillator of the predator–prey type.[6] A predator–prey chemical oscillator was theoretically proposed by McCaskill and co-workers in 1998[7] together with a tentative experimental implementation based on transcription and reverse transcription.[8] However, no oscillations or waves were reported. Beyond purely chemical phenomena, predator–prey dynamics are ubiquitous in ecology.[9a] Balagaddé and collaborators[9b] implemented an ecosystem based on a kill-and-rescue mechanism. Oscillations in the populations of two engineered strains of bacteria were observed, lasting for 1.5 periods. Nevertheless, both the mechanism and the need for a delay introduced by transcription to observe oscillations suggest that an activator–inhibitor model rather than a predator–prey model better describes the dynamics of their system. Predator–prey traveling waves have been experimentally observed in the wild in oceanic plankton[10] and vegetation,[11] but field experiments are difficult to carry out. While Bauer and collaborators have experimentally observed traveling concentration fronts in the Q-β replicase system,[12] the present report is to the best of our knowledge the first to describe the synthesis and observation of predator–prey waves in the laboratory.

■ EXPERIMENTAL SECTION

Reaction Assembly and Monitoring. The reaction buffer contained 20 mM Tris-HCl, 10 mM $(NH_4)_2SO_4$, 10 mM KCl, 50 mM NaCl, 8 mM $MgSO_4$, 400 μM of each dNTP [New England Biolabs (NEB)], 0.1% Synperonic F108 (Aldrich), 5 ng/μL extremely thermostable single-stranded binding protein (ETSSB) (NEB), 500 μg/mL BSA (NEB), 2 μM Netropsin (Sigma-Aldrich), and 4 mM dithiothreitol and had a pH of 8.8. If necessary, 1× EvaGreen (Biotium) was added (20-fold dilution of the manufacturer's stock solution). The DNA oligonucleotides [prey (N), predator (P), and prey template (G)] were purchased with HPLC purification (Biomers) and quantified by UV absorption. Their sequences were the following: (N) 5′-CATTCGGCCG-3′; (P) 5′-CATTCGGCCGAATG-3′; and (G) 5′-C*G*G*CCGAATGCGGCCGAATG-3′, where the asterisks indicate phosphorothioate groups. Three enzymes were further added to the reaction mixture: Bst DNA polymerase (pol), Nb.BsmI nicking enzyme (nick), and ttRecJ exonuclease (exo); pol and nick were obtained from NEB, and exo was a kind gift of R. Masui. The concentration of nick was 500 units/mL, but its activity severely changed from batch to batch. Therefore, it was monitored with an independent assay, and its final concentration was modified accordingly. The concentrations of N, P, G, pol, and exo were varied slightly between experiments as specified below. Further details are provided in ref 6. Typically, 40 μL of a reaction mixture containing the reaction buffer, N, P, G, and the enzymes was assembled, and 20 μL of this mixture was introduced into a reactor made with two punched Parafilm layers between two glass cover slides [Figure S1 in the Supporting Information (SI)]. The reactor was sealed by heating it for 10 s at 50 °C. It was then monitored at 44.0 or 44.5 °C (see below) in an Olympus IX71 inverted microscope equipped with a transparent heating plate (Tokai-Hit) using a 1× objective, LED illumination (CoolLED), and an iXon3 897 EM-CCD camera (Andor). Images were acquired using the open-source microscopy software μManager 1.4[13] and treated with ImageJ (NIH). The rest of the reaction mixture was monitored in 150 μL polymerase chain reaction (PCR) tubes in a CFX or MiniOpticon real-time PCR machine (Biorad) as a zero-dimensional (0D) (well-mixed) control experiment.

Simulations. The simulations in Figure 3 were performed by integrating eqs 1−6 in 1D in Mathematica (Wolfram) using the method of lines. The domain of integration was 0 to 11 mm in space and 0 to 600 min in time. Space was discretized into at least 100 cells. The symmetry was broken by choosing exponential initial conditions for P ($10^{-x+1} + 10$) and N (10^{-x-3}). Boundary conditions with zero concentration gradient were chosen for P and N. A small constant leak set at $10^{-5}k_1 \cdot pol \cdot G$ (where pol and G denote the concentrations of pol and G, respectively) was introduced into eq 1 to take into account the nonspecific reaction of pol with G in the absence of N.[14] This leak also helped to avoid convergence problems.

■ RESULTS AND DISCUSSION

Predator−Prey Reaction Mechanism. The reaction mechanism is depicted in Figure 1. The information concerning prey growth is stored in a 20-base single-stranded DNA (ssDNA) denoted by G (for "Grass"). G is composed of a four-base domain $a*$ and a six-base domain b, where $a*$ is the complement of a and b is self-complementary. G has the sequence 5′-$ba*ba*$-3′ and serves as a template for the growth of the prey, N, a 10-mer of sequence ab. Prey growth proceeds as follows: N hybridizes to the 3′ end of G to form the complex G:N, which is extended by a polymerase (pol) to yield the double strand I_N. I_N bears a recognition site for a nicking enzyme (nick), which cuts its top (prey) strand into two equal parts, yielding two copies of N upon dehybridization.
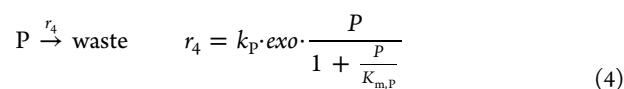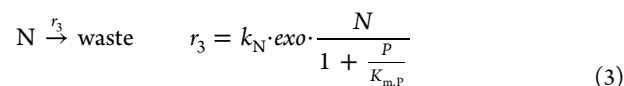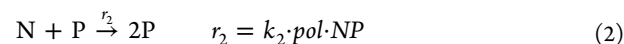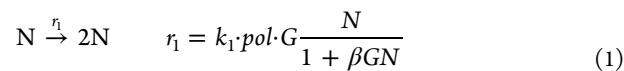
The predator, P, is a palindromic 14-base ssDNA with sequence $aba*$. During predation, N hybridizes over P, and pol extends this adduct to form the double strand P:P. Upon dehybridization, P:P yields two copies of P. The two active
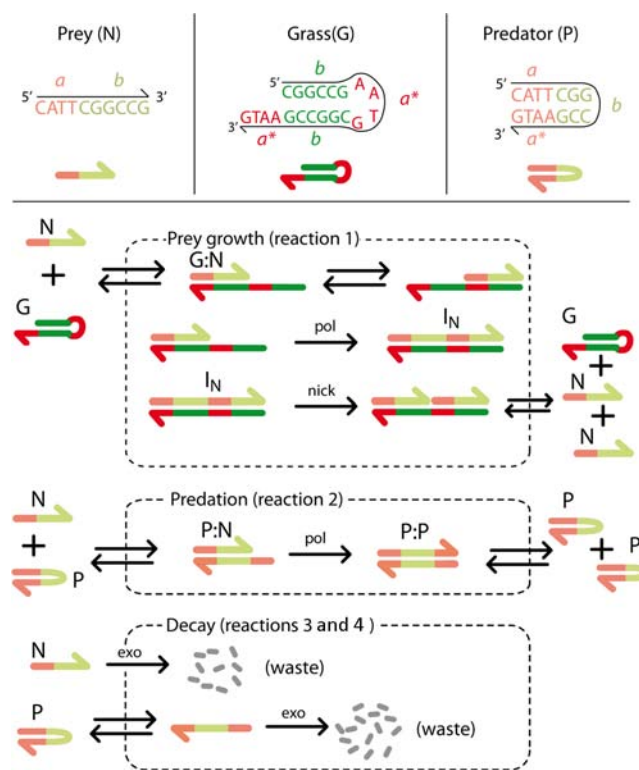
Figure 1. Mechanism of the molecular predator−prey network. N, P, and G denote the prey, the predator, and the template on which the prey grows, respectively. Harpoon-ended arrows denote DNA strands. Double arrows correspond to DNA hybridization/dehybridization reactions, whereas single arrows indicate irreversible enzymatic transformations. Complementary DNA domains have the same color: red for a and its complement $a*$ and green for b, which is self-complementary. Light and dark hues indicate strands that can and cannot be degraded by the exonuclease (exo), respectively. The polymerase and nicking enzyme are denoted as pol and nick, respectively.

species N and P are degraded to unreactive dNMPs by a 5′→3′ processive, ssDNA-specific exonuclease (exo). G is not digested because it bears three protective phosphorothioate modifications at the 5′ end. The reaction is performed around 44 °C, where the 20-base-pair I_N intermediate is stable but the 10-base-pair G:N is not (T_m = 64 and 43 °C, respectively, at 100 nM[15]).

Two of us recently demonstrated that the following simplified mechanism can accurately account for this process:[6]

$$N \xrightarrow{r_1} 2N \qquad r_1 = k_1 \cdot pol \cdot G \frac{N}{1 + \beta GN} \tag{1}$$

$$N + P \xrightarrow{r_2} 2P \qquad r_2 = k_2 \cdot pol \cdot NP \tag{2}$$

$$N \xrightarrow{r_3} \text{waste} \qquad r_3 = k_N \cdot exo \cdot \frac{N}{1 + \frac{P}{K_{m,P}}} \tag{3}$$

$$P \xrightarrow{r_4} \text{waste} \qquad r_4 = k_P \cdot exo \cdot \frac{P}{1 + \frac{P}{K_{m,P}}} \tag{4}$$

Prey growth (eq 1) and degradation of prey (eq 3) and predator (eq 4) obey Michaelis−Menten kinetics, while predation (eq 2) follows mass-action kinetics. In these equations, r_i is the rate of reaction i; k_1, k_2, k_N and k_P are the

rate constants for prey growth, predation, prey decay, and predator decay, respectively; *pol*, *exo*, and *G* are the total concentrations of pol, exo, and G, respectively; N and P are the concentrations of N and P, respectively, at time *t*; $K_{m,P}$ is the Michaelis–Menten constant for the saturation of exo by P; and β is a parameter that takes into account the saturation of the prey growth. These rate laws were obtained experimentally and are valid for a range of concentrations and time scales comparable to those used in our experiments. In particular, a Michaelis–Menten term was needed to account for the saturation by N during prey growth but was not needed for P during predation. This suggests that the saturation term is mostly due to the nicking enzyme, which is not needed for predation. Similarly, for the exonuclease, a saturation term was needed for P but not for N. For a thorough discussion of the kinetic model, see the Supporting Information for ref 6.

In a well-stirred reactor, where diffusion can be neglected, the following dynamics can be observed, depending on the experimental conditions: extinction of both species, prey-only steady state, sustained oscillations, and damped oscillations followed by stable coexistence of predators and preys. Oscillations have typical periods in the 80–300 min range, depending on the concentrations of G and the enzymes and on the temperature. Because the system contains an internal energy source (dNTP) and sink (exo), these dynamics can be observed in a closed tube. In the following, we characterize the spatiotemporal dynamics of this predator–prey (PP) molecular system in a spatially extended (and closed) reactor.

Prey Waves. Figure 2 displays a traveling wave of preys moving from left to right in an unstirred, closed circular reactor containing the PP system. The reactor was 8 mm in diameter and 200 μm thick. Concentration changes were followed through the yellow fluorescence of a DY530 dye attached to the 3′ end of G. When a DNA strand hybridizes over G, the fluorescence of the dye is reduced through N-quenching.[3e,16] Therefore, the yellow fluorescence intensity shift reports primarily on the concentration of the prey species.

Prey waves appeared as follows. Starting from a reactor with initially homogeneous concentrations and depending on the experimental conditions, zero, one, or two first homogeneous oscillations of the prey concentration were observed. Subsequently, the spatial symmetry was broken, most often on the borders of the reactor, and the concentration of prey started to grow within a small zone (Figure 2 left, top panel). When this zone reached a size of about 2 mm, it detached from the border, and a wave of prey started to travel from left to right. The wave shown in Figure 2 corresponds to the sixth oscillation of the PP system after the beginning of the reaction. It traveled with a velocity of 80 μm min^{-1}, and its width at half height was 2 mm. When either two prey fronts collided or one front reached the border of the reactor, the wave vanished, the yellow fluorescence shift became homogeneous again, and a subsequent wave of prey was generated. This process happened with a periodicity of 110 ± 10 min in the experiment corresponding to Figure 2, resulting in a wavelength of 9 ± 1 mm.

Predators Follow Preys. Under the above experimental conditions, only the prey produced a significant fluorescence signal. However, in PP dynamics we expect a band of predators to follow the prey front in the so-called "waves of pursuit and evasion" situation.[17] To reveal this phenomenon, we added a second fluorescent dye, EvaGreen, to the reaction mixture. The green fluorescence of this nonspecific dsDNA intercalator has
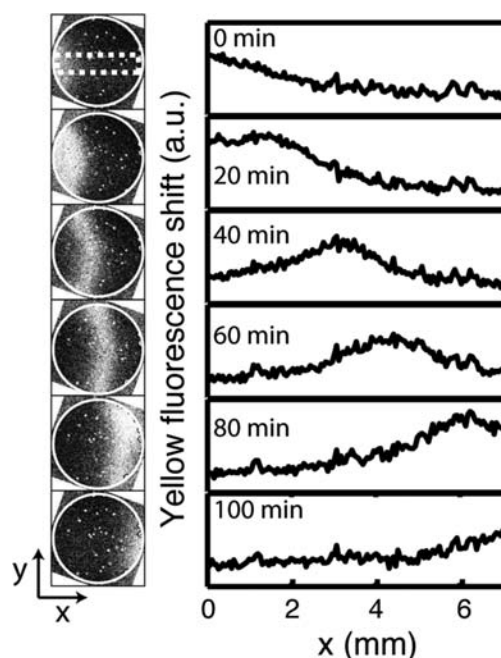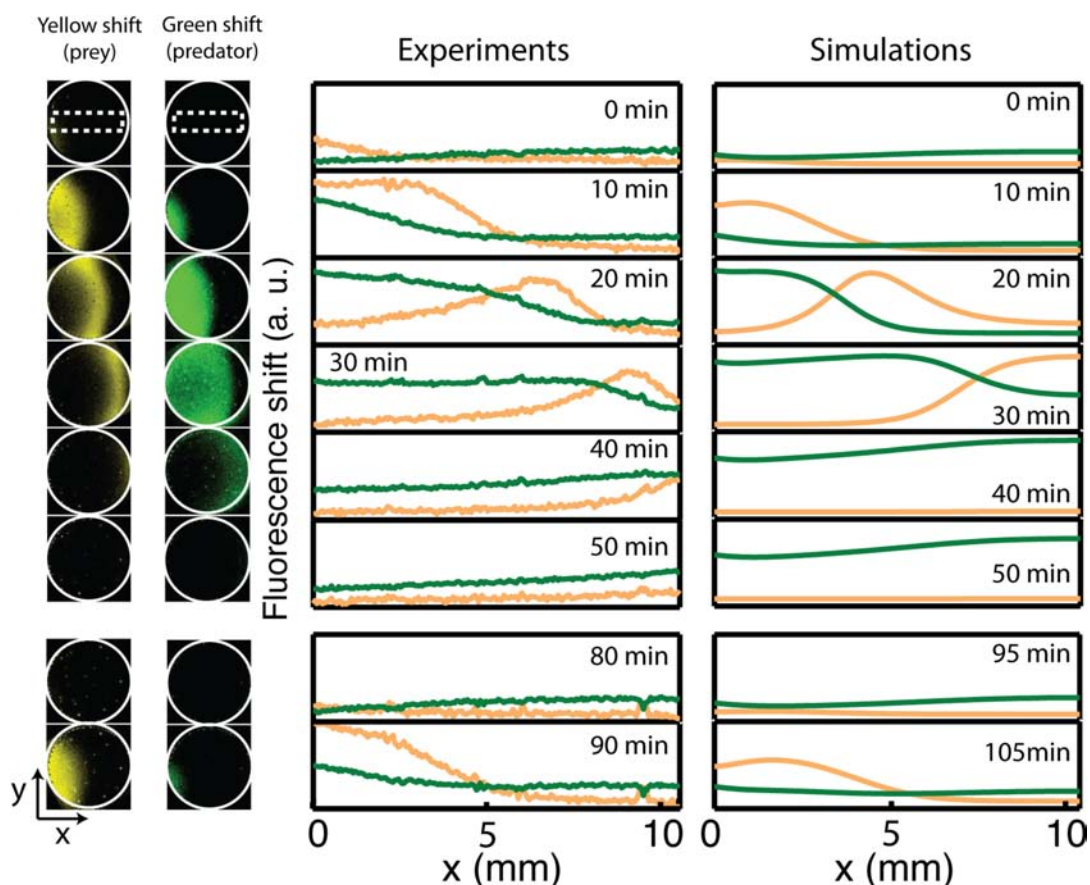

Figure 2. Traveling wave of preys in a predator–prey molecular landscape. (left) Time-lapse images of the yellow fluorescence shift taken every 20 min in an 8 mm diameter, 200 μm thick circular reactor. The borders of the reactor are highlighted in white. (right) Corresponding yellow fluorescence intensity shift profiles along *x*. The fluorescence was measured in the white dotted rectangle shown in the top left panel. The initial conditions were homogeneous with 10 nM P and 10 nM N, with T = 44.5 °C, *pol* = 1.6 nM, *exo* = 25 nM, and G = 110 nM. Here *t* = 0 min corresponds to 535 min after the start of the experiment (see movie S1 in the SI).

been shown to account principally for the concentration of predators.[6]

Indeed, Figure 3 clearly shows that the front of the yellow fluorescence shift, indicating high prey concentration, was followed by a front of green fluorescence shift due to the predator. The predator wave started to grow at the same location as the prey wave (on the left side of the reactor in Figure 3) but with a 4 min delay (movie S2 in the SI). Here the prey wave was 3 mm wide at half height, while the predator wave was at least as large as the reactor size (11 mm). When the prey wave hit the right side of the reactor, the predator concentration decreased nearly homogeneously (as the predator was consumed by the exonuclease) until its value reached a minimum, and then the cycle started again. The two waves moved at the same velocity, here 320 μm min^{-1}. The difference with the value in Figure 2 is attributed to the presence of the DNA-intercalating dye, which modified the kinetics. Such waves repeated several times (six pulses in the experiment of Figure 2, seven in the experiment of Figure 3) before the system died out.

With eqs 1–6, a 1D reaction–diffusion simulation was performed to test the validity of the model (Figure 3 right; see below for equations and parameter determination). The shapes, widths, and velocities of the prey and predator pulses were in good agreement with experimental results. The period of the oscillations appeared to be 10% longer in the simulations. The degradation of predators was significantly slower in the simulations compared with the experiments (Figure 3, *t* = 50 min). In view of the simplicity of the two-variable model, the

Figure 3. A wave of predators follows the wave of preys in a predator−prey molecular network. (left) Time-lapse images of the fluorescence shifts in the yellow channel (corresponding to the prey concentration) and the green channel (corresponding to the predator concentration), taken every 10 min in an 11 mm diameter, 200 μm thick circular reactor. The borders of the reactor are highlighted in white. Here t = 0 min corresponds to 438 min after the start of the experiment (see movie S2 in the SI). (middle) Profiles along x of the yellow (prey) and green (predator) fluorescence shifts corresponding to the images on the left, averaged in the white dotted rectangles. Initial conditions were homogeneous with 15 nM P and 5 nM N, with T = 44.5 °C, pol = 1.7 nM, exo = 25 nM, G = 140 nM, and 1× EvaGreen. (right) 1D reaction−diffusion simulations of the normalized prey (yellow) and predator (green) concentrations using eqs 1−6 and the parameters described in the text.

good agreement between the experiments and simulations is striking.

To assess the kinematic behavior of each pulse, we plotted the profile of the yellow fluorescence shift across the reaction chamber (x axis) as a function of time for the whole experiment shown in Figure 3, which lasted 10 h (Figure 4). The white stripes in Figure 4A correspond to pulses of high prey concentration traveling across the reactor. Pulses 1 and 2 are nearly vertical, indicating that the speeds of these traveling waves were very high; these pulses account for the nearly homogeneous first two oscillations (movie S2 in the SI). For pulses 3−9, we can distinguish an initial phase with nearly infinite velocity (in a region corresponding to x < 3 mm) where the prey concentration grew without moving. During this time and in this area of the reactor, homogeneous growth was faster than the traveling velocity of the spatial instability and thus dominated the dynamics. After this initial phase, the pulse position versus time could be fitted to a straight line (i.e. the pulse traveled at constant velocity). Figure 4B shows the fitted velocity for each pulse. We observe that after pulse 3, the velocity settled around a roughly constant value of 380 ± 80 μm/min, indicating convergence to pseudostationary behavior (true stationary behavior cannot be expected in this closed system because the energy source, dNTP, is bound to fade out).
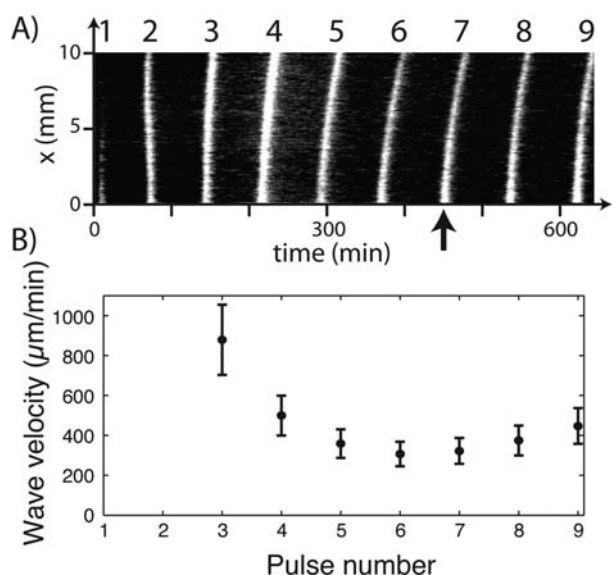
Analytical Calculation of the Wave Velocity. Traveling waves of constant velocity are classical solutions of a two-species, predator−prey reaction−diffusion system. Because the PP reaction network considered here was constructed from simple enzymatic and hybridization reactions, it was possible to propose the mechanism described in eqs 1−4. We subsequently used this information to derive an analytical expression for the wave velocity of predators following Murray[17] and Dunbar.[18] We can write the reaction−diffusion problem of the PP system in 1D as follows:

$$\frac{\partial N}{\partial t} = r_1 - r_2 - r_3 + D_N \frac{\partial^2 N}{\partial x^2} \tag{5}$$

$$\frac{\partial P}{\partial t} = r_2 - r_4 + D_P \frac{\partial^2 P}{\partial x^2} \tag{6}$$

where D_i is the diffusion coefficient of species i. For convenience, eqs 5 and 6 were expressed in dimensionless form in terms of the variables $n = N/K_{m,P}$ and $p = P/K_{m,P}$:

$$\frac{\partial n}{\partial T} = g\frac{n}{1 + Bgn} - pn - \lambda\delta\frac{n}{1 + p} + \frac{\partial^2 n}{\partial X^2} \tag{7}$$

14589

dx.doi.org/10.1021/ja403584p | *J. Am. Chem. Soc.* 2013, 135, 14586−14592

Figure 4. The velocity of the waves is constant after an initial phase of homogeneous growth. (A) Kymogram of the yellow fluorescence shift along x at different times for the predator–prey system in Figure 3. The numbers at the top refer to the pulse numbers since the beginning of the experiment. For comparison, the data in Figure 3 were extracted at the time stamp signaled by the arrow. (B) Wave velocity after the initial phase of homogeneous growth for each pulse in (A). Error bars correspond to one standard deviation of the linear fit.

$$\frac{\partial p}{\partial T} = np - \delta\frac{p}{1+p} + d\frac{\partial^2 p}{\partial X^2} \qquad (8)$$

where $T = t/t_c$ and $X = x/x_c$, in which $t_c = (k_2 \cdot pol \cdot K_{m,P})^{-1}$ and $x_c = (D_N t_c)^{1/2}$; $g = k_1 G/k_2 K_{m,P}$, $B = \beta k_2 K_{m,P}^2/k_1$, $\lambda = k_N/k_P$, $\delta = (rec/pol)(k_P/k_2 K_{m,P})$, and $d = D_P/D_N$. We expect the leading edge of the prey wave to advance in a zone with low concentration of both prey and predators. Setting $n \ll (gB)^{-1}$ and $p \ll 1$ with $p \ll n$, we may develop eqs 7 and 8 to second order in n and first order in p, yielding

$$\frac{\partial n}{\partial T} \approx An\left(1 - \frac{n}{K}\right) - (1 - \lambda\delta)pn + \frac{\partial^2 n}{\partial X^2} \qquad (9)$$

$$\frac{\partial p}{\partial T} \approx np - \delta p + d\frac{\partial^2 p}{\partial X^2} \qquad (10)$$

where $A = g - \lambda\delta$ and $K = (g - \lambda\delta)/Bg^2$. One may recognize a predator–prey model where the prey growth follows a logistic equation with carrying capacity K. Dunbar has proved that for equations such as eqs 9 and 10 there exist traveling-wave solutions with the minimal velocity

$$v = 2C\sqrt{D_P k_2 \cdot pol \cdot K_{m,P}} \qquad (11)$$

where $C = \{[(g - \lambda\delta)/Bg^2] - \delta\}^{-1/2}$ is a nondimensional constant on the order of unity. From the theoretical standpoint, eq 11 has to be considered with caution because we have approached the velocity of a periodic wave with that of a solitary front. In the first case, the system of ordinary differential equations for the moving frame associated with eqs 5 and 6 contains a limit-cycle trajectory. In the second case, the trajectory connects two steady states.

Numerical values for the parameters were reported in ref 6, where the same PP system was considered. To account for the slightly different conditions used here (temperature and

enzyme batch activity), these values were refined by direct fitting of the fluorescence record of the same reactive mix incubated in a control 0D (tube) experiment with eqs 5 and 6 in the absence of diffusion (Figure S2 in the SI). We obtained $k_1 = 3 \times 10^{-3}$ nM^{-2} min^{-1}, $k_2 = 4 \times 10^{-3}$ nM^{-2} min^{-1}, $k_N = 10^{-2}$ nM^{-1} min^{-1}, $k_P = 4 \times 10^{-3}$ nM^{-1} min^{-1}, $\beta = 6 \times 10^{-5}$ nM^{-2}, and $K_{m,P} = 34$ nM. We used $pol = 1.7$ nM, $exo = 25$ nM, and $G = 140$ nM. Calculating the diffusion coefficient of P as a seven-base-pair dsDNA using the empirical law at 20 °C proposed by Stellwagen et al.[19] [$D = (7.73 \times 10^{-10}$ m^2 s$^{-1})$ $n_{bp}^{-0.67}$, where n_{bp} is the number of base pairs] and correcting for the temperature gave $D_P = 2 \times 10^4$ μm^2 min^{-1}. This yielded $C = 1.3$, from which the minimal velocity of the front of traveling waves in our system was $v \approx 170$ μm min^{-1}, which is in good agreement with the velocity of 350 μm min^{-1} measured in Figure 3B. For comparison, a similar set of parameters extracted from the experiment in Figure 2 yielded $v \approx 160$ μm min^{-1}, while we measured 80 μm min^{-1}. Equation 11 thus provides a simple analytical expression for the velocity of the front that is correct within a factor of 2. There are at least two reasons to explain this difference. The presence of EvaGreen in one of the experiments can modify the rate constants[3d] by as much as a factor 10. Furthermore, eq 11 was derived for an infinite one-dimensional reactor, while the experiments were performed in a finite 2D reactor.

Spiral Waves. When the initial conditions were inhomogeneous in prey, we observed more complex patterns, such as spirals (movie S3 in the SI) and target patterns (movie S4 in the SI) with striking phenomena of wave annihilation when two traveling fronts collided. Figure 5 shows time-lapse images of the yellow fluorescence shift for our PP system with inhomogeneous initial conditions of prey. To create these
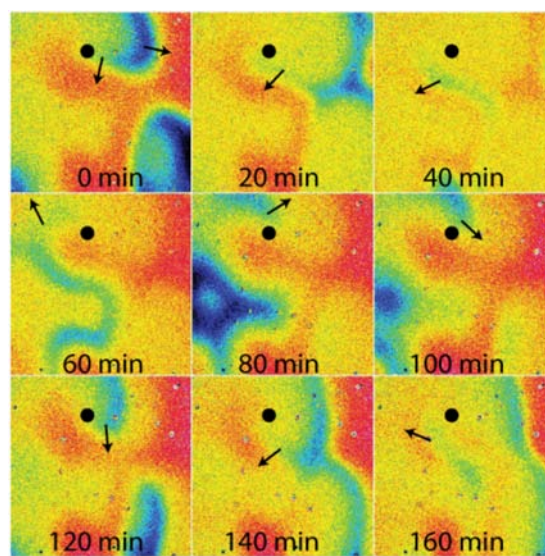
Figure 5. Clockwise-rotating spiral of preys. Time-lapse, false-color yellow fluorescence shift images of the PP system with initial prey concentration localized on the bottom left and top right corners. The initial predator was homogeneous at a concentration of 10 pM. Blue and red represent high and low prey concentrations, respectively. To guide the eye, the black dot indicates the rotor of the spiral and the arrows show the direction of the propagating wave. Images were taken every 20 min starting 784 min after the beginning of the experiment. The scale bar is 2 mm. $T = 44$ °C, $pol = 1.6$ nM, $exo = 15$ nM, and $G = 140$ nM (see movie S3).

conditions, we dried 0.1 pmol of prey on two spots about 1 mm in diameter in the bottom left and top right corners of a 10 mm wide square chamber. We expected that the redissolution of these spots after the reactor assembly would provide an initially inhomogeneous concentration profile for the prey that would vanish after the first oscillation. In this experiment, fronts of preys emitted by the spots in all directions were first observed (movie S3). These waves later generated more complex traveling patterns when colliding with each other and the reactor walls. After about six periods of oscillation, a spiral pattern with a single arm was observed that lasted for four rotation periods of 140 ± 10 min.

Throughout this paper we have described the observed waves as reaction–diffusion waves: for the wave to propagate, matter has to be transported across space. These waves are thus capable of carrying information. Waves in chemical systems can also arise through a totally different mechanism that does not involve the transport of matter. This second type of wave is called a phase wave and arises when contiguous chemical oscillators are slightly out of phase, for example as a result of a small thermal gradient. Spiral waves cannot arise through this second mechanism. Moreover, the waves observed here could travel around impermeable walls (Figure S3 in the SI). These two observations indicate that the waves described here are indeed reaction–diffusion waves.

CONCLUSION

The first chemical waves were observed experimentally by Zaikin and Zhabotinsky in 1970[20] in the Belousov–Zhabotinsky (BZ) reaction. Spirals were soon observed by Winfree,[21] leading to a large body of experimental and theoretical work on dissipative chemical structures.[22] These spatiotemporal patterns were obtained from a handful of preexisting reaction networks whose parameters were typically controlled via the concentrations of some of the species involved. Eventually, to observe Turing patterns, an additional layer of control targeting the diffusion coefficients had to be implemented.[23] Here we have shown for the first time the synthesis of traveling waves and spiral patterns in a chemical network engineered from the bottom up using synthetic nucleic acids and standard enzymatic reactions. We expect that this approach will provide an instrumental answer to the long-standing problem of out-of-equilibrium chemical patterning, that is, the great difficulty of tuning the control parameters of the underlying chemical network. The ideal approach would provide control of not only the reactivity and the diffusion coefficients of each species but also, and most importantly, their connectivity pattern (the topology of the network). In nucleic acid networks, the ease with which these features can be rationally designed[3d,24] should bring unprecedented opportunities for assaying the principles of spatiotemporal order formation in chemistry. Moreover, nucleic acids are extremely versatile chemical compounds[25] with structural, mechanical, recognition, catalytic, and information-processing capabilities exemplified, respectively, by DNA origami,[26] DNA gels,[27] aptamers,[28] ribozymes,[29] and DNA-based logic circuits.[3c,24a,30] This opens the route to applications where the self-organized pattern would control downstream processes.

The system reported here is also remarkable because it shows pseudostationnary behavior in a closed reactor. Indeed, only three chemical systems display this specific feature: the BZ reaction with its microemulsion derivative, the chlorite–iodide–malonic acid (CIMA) reaction, and the ferrocyanide–iodide–sulfite reaction.[31] The ability to work in a closed reactor opens up not only facilitated but also specific experimental possibilities, such as the use of arrays of microscopic compartments.[32]

ASSOCIATED CONTENT

S Supporting Information

Movies S1, S2, and S3 (corresponding to Figures 2, 3, and 5 in the main text) as well as movie S4 and Figures S1−S3. This material is available free of charge via the Internet at http://pubs.acs.org.

AUTHOR INFORMATION

Corresponding Author

aestevez@lpn.cnrs.fr; rondelez@iis.u-tokyo.ac.jp

Notes

The authors declare no competing financial interest.

REFERENCES

(1) (a) Gregor, T.; Bialek, W.; van Steveninck, R. R. R.; Tank, D. W.; Wieschaus, E. F. *Proc. Natl. Acad. Sci. U.S.A.* **2005**, *102*, 18403−18407. (b) Kondo, S.; Miura, T. *Science* **2010**, *329*, 1616−1620. (c) Economou, A. D.; Ohazama, A.; Porntaveetus, T.; Sharpe, P. T.; Kondo, S.; Basson, M. A.; Gritli-Linde, A.; Cobourne, M. T.; Green, J. B. A. *Nat. Genet.* **2012**, *44*, 348−351.

(2) (a) Gunawardena, J. Models in Systems Biology: The Parameter Problem and the Meanings of Robustness. In *Elements of Computational Systems Biology*; Wiley: Hoboken, NJ, 2010; pp 19−47. (b) Phillip, Y.; Kiss, V.; Schreiber, G. *Proc. Natl. Acad. Sci. U.S.A.* **2012**, *109*, 1461−1466.

(3) (a) Seelig, G.; Soloveichik, D.; Zhang, D. Y.; Winfree, E. *Science* **2006**, *314*, 1585−1588. (b) Soloveichik, D.; Seelig, G.; Winfree, E. *Proc. Natl. Acad. Sci. U.S.A.* **2010**, *107*, 5393−5398. (c) Qian, L.; Winfree, E. *Science* **2011**, *332*, 1196−1201. (d) Montagne, K.; Plasson, R.; Sakai, Y.; Fujii, T.; Rondelez, Y. *Mol. Syst. Biol.* **2011**, *7*, No. 466. (e) Padirac, A.; Fujii, T.; Rondelez, Y. *Nucleic Acids Res.* **2012**, *40*, No. e118. (f) Padirac, A.; Fujii, T.; Rondelez, Y. *Proc. Natl. Acad. Sci. U.S.A.* **2012**, *109*, E3212−E3220. (g) Shin, J.; Noireaux, V. *ACS Synth. Biol.* **2011**, *1*, 29−41.

(4) (a) Estevez-Torres, A.; Le Saux, T.; Gosse, C.; Lemarchand, A.; Bourdoncle, A.; Jullien, L. *Lab Chip* **2008**, *8*, 1205−1209. (b) Estevez-Torres, A.; Gosse, C.; Le Saux, T.; Allemand, J. F.; Croquette, V.; Berthoumieux, H.; Lemarchand, A.; Jullien, L. *Anal. Chem.* **2007**, *79*, 8222−8231.

(5) Allen, P.; Chen, X.; Ellington, A. *Molecules* **2012**, *17*, 13390−13402.

(6) Fujii, T.; Rondelez, Y. *ACS Nano* **2013**, *7*, 27−34.

(7) Ackermann, J.; Wlotzka, B.; McCaskill, J. S. *Bull. Math. Biol.* **1998**, *60*, 329−354.

(8) Wlotzka, B.; McCaskill, J. S. *Chem. Biol.* **1997**, *4*, 25−33.

(9) (a) Bauer, G. J.; McCaskill, J. S.; Otten, H. *Proc. Natl. Acad. Sci. U.S.A.* **1989**, *86*, 7937−7941. (b) McCaskill, J. S.; Bauer, G. J. *Proc. Natl. Acad. Sci. U.S.A.* **1993**, *90*, 4191−4195.

(10) Wyatt, T. *Mar. Biol.* **1973**, *22*, 137−158.

(11) Lejeune, O.; Tlidi, M. *J. Veg. Sci.* **1999**, *10*, 201−208.

(12) (a) Turchin, P. *Complex Population Dynamics: A Theoretical/Empirical Synthesis*; Princeton University Press: Princeton, NJ, 2003.

(b) Balagaddé, F. K.; Song, H.; Ozaki, J.; Collins, C. H.; Barnet, M.; Arnold, F. H.; Quake, S. R.; You, L. *Mol. Syst. Biol.* **2008**, *4*, No. 187.

(13) Edelstein, A.; Amodaj, N.; Hoover, K.; Vale, R.; Stuurman, N. *Computer Control of Microscopes Using μManager*; Wiley: Hoboken, NJ, 2010.

(14) Tan, E.; Erwin, B.; Dames, S.; Ferguson, T.; Buechel, M.; Irvine, B.; Voelkerding, K.; Niemz, A. *Biochemistry* **2008**, *47*, 9987−9999.

(15) (a) Zuker, M. *Nucleic Acids Res.* **2003**, *31*, 3406−3415. (b) SantaLucia, J., Jr. *Proc. Natl. Acad. Sci. U.S.A.* **1998**, *95*, 1460−1465.

(16) Marras, S. A. E.; Kramer, F. R.; Tyagi, S. *Nucleic Acids Res.* **2002**, *30*, No. e122.

(17) Murray, J. D. *Mathematical Biology II: Spatial Models and Biomedical Applications*; Springer: New York, 2003.

(18) (a) Dunbar, S. R. *Trans. Am. Math. Soc.* **1984**, *286*, 557−594. (b) Dunbar, S. R. *J. Math. Biol.* **1983**, *17*, 11−32.

(19) Stellwagen, E.; Lu, Y. J.; Stellwagen, N. C. *Biochemistry* **2003**, *42*, 11745−11750.

(20) Zaikin, A. N.; Zhabotinsky, A. M. *Nature* **1970**, *225*, 535−537.

(21) Winfree, A. T. *Science* **1972**, *175*, 634−636.

(22) Epstein, I.; Pojman, J. A. *An Introduction to Nonlinear Chemical Reactions*; Oxford University Press: New York, 1998.

(23) (a) Castets, V.; Dulos, E.; Boissonade, J.; De Kepper, P. *Phys. Rev. Lett.* **1990**, *64*, 2953−2956. (b) Ouyang, Q.; Swinney, H. L. *Nature* **1991**, *352*, 610−612.

(24) (a) Zhang, D. Y.; Seelig, G. *Nat. Chem.* **2011**, *3*, 103−113. (b) Zhang, D. Y.; Winfree, E. *J. Am. Chem. Soc.* **2009**, *131*, 17303−17314.

(25) Pinheiro, V. B.; Taylor, A. I.; Cozens, C.; Abramov, M.; Renders, M.; Zhang, S.; Chaput, J. C.; Wengel, J.; Peak-Chew, S.-Y.; McLaughlin, S. H.; Herdewijn, P.; Holliger, P. *Science* **2012**, *336*, 341−344.

(26) Rothemund, P. W. K. *Nature* **2006**, *440*, 297−302.

(27) Bertrand, O. J. N.; Fygenson, D. K.; Saleh, O. A. *Proc. Natl. Acad. Sci. U.S.A.* **2012**, DOI: 10.1073/pnas.1208732109.

(28) (a) Ellington, A. D.; Szostak, J. W. *Nature* **1990**, *346*, 818−822. (b) Tuerk, C.; Gold, L. *Science* **1990**, *249*, 505−510.

(29) Herschlag, D.; Cech, T. R. *Biochemistry* **1990**, *29*, 10159−10171.

(30) (a) Stojanovic, M. N.; Mitchell, T. E.; Stefanovic, D. *J. Am. Chem. Soc.* **2002**, *124*, 3555−3561. (b) Ran, T.; Kaplan, S.; Shapiro, E. *Nat. Nanotechnol.* **2009**, *4*, 642−648.

(31) Vanag, V. K.; Epstein, I. R. *Int. J. Dev. Biol.* **2009**, *53*, 673−681.

(32) (a) Toiya, M.; Vanag, V.; Epstein, I. *Angew. Chem., Int. Ed.* **2008**, *47*, 7753−7755. (b) Taylor, A. F.; Tinsley, M. R.; Wang, F.; Huang, Z.; Showalter, K. *Science* **2009**, *323*, 614−617.